New Journal of Physics
The open access journal at the forefront of physics

Deutsche Physikalische Gesellschaft DPG IOP Institute of Physics

PAPER • OPEN ACCESS

Time-delayed feedback control of the Dicke–Hepp–Lieb superradiant quantum phase transition

To cite this article: Wassilij Kopylov *et al* 2015 *New J. Phys.* **17** 013040

New Journal of Physics
The open access journal at the forefront of physics

Deutsche Physikalische Gesellschaft DPG
IOP Institute of Physics

Published in partnership with: Deutsche Physikalische Gesellschaft and the Institute of Physics

OPEN ACCESS

RECEIVED
11 August 2014

ACCEPTED FOR PUBLICATION
8 December 2014

PUBLISHED
20 January 2015

PAPER

Time-delayed feedback control of the Dicke–Hepp–Lieb superradiant quantum phase transition

Wassilij Kopylov[1], **Clive Emary**[2], **Eckehard Schöll**[1] **and Tobias Brandes**[1]

[1] Institut für Theoretische Physik, Technische Universität Berlin, D-10623 Berlin, Germany
[2] Department of Physics and Mathematics, University of Hull, UK

E-mail: kopylov@itp.tu-berlin.de

Keywords: Dicke model, time-delayed feedback, Pyragas control, quantum phase transitions, quantum optics

Abstract

We apply the time-delayed Pyragas control scheme to the dissipative Dicke model via a modulation of the atom-field-coupling. The feedback creates an infinite sequence of non-equilibrium phases with fixed points and limit cycles in the primary superradiant regime. We analyse this Hopf bifurcation scenario as a function of delay time and feedback strength and determine analytical conditions for the phase boundaries.

1. Introduction

Interacting quantum systems with time-dependent Hamiltonians offer rich and exciting possibilities to study many-body physics beyond equilibrium conditions. There has been a recent surge in generating correlated non-equilibrium dynamics in a controlled way by changing the interaction parameters as a function of time, for example, by periodically modulating the coupling constants or by abruptly quenching them. Of particular interest then is the fate of coherent quantum dynamics and phase transitions in such scenarios. Indeed, intriguing phenomena have been discussed, such as coherent control of tunnelling in Bose–Einstein condensates [1], thermalization after quenches [2], or dynamical and excited state quantum phase transitions [3, 4].

In this paper, we show another and conceptually very different option for driving quantum systems out of equilibrium, i.e., by modulating interaction parameters via a measurement-based feedback loop. The time-delayed Pyragas control scheme [5] that we propose here has been successfully employed in a classical context over the past twenty years, for example, as a tool to stabilize certain orbits in chaotic systems or networks [6–9]. Its key idea is to feed back the difference between two signals of the same observable at different times, such that a stabilization occurs when the delay time matches an intrinsic period of the dynamical system.

Our key idea is to generate new non-equilibrium phases via Pyragas control of the interaction between the single bosonic cavity mode and the collection of quantum two-level systems [10] in Dicke–Hepp–Lieb superradiance. The superradiant transition without control, which has been observed only recently in cold atoms within a photonic cavity [11–14], also with applied quenches [15] or using cavity-assisted Raman transitions [16], has an underlying semi-classical bifurcation, which makes it an ideal candidate to study feedback at the boundary between non-linear (classical) dynamics and quantum many-body systems [17].

Open loop control of the Dicke model has been studied in the past, for example, in the form of periodic modulations of the atom-field-coupling constants [13, 18] or the level splitting modulation [19, 20]. Recently, Grimsmo *et al* [21] found a speed-up towards the stationary state and qualitative changes of the phase diagram when applying Pyragas-feedback to the cavity mode alone incoherently. In our model, we condition the effective coupling strength between the cavity and the atoms of the Dicke system—in the experiment just proportional to the laser intensity [11]—on a difference of photon numbers emitted from the cavity at different times. We use a mean field approach and linear stability analysis in order to show that closed loop control dramatically affects the states in the primary superradiant regime, creating a new phase with an infinite sequence of Hopf bifurcations

between stable fixed points and limit cycles. We also derive analytical results in the form of a single transcendental equation that determined the boundaries between the different zones in the phase diagrams.

The structure of this paper is as follows: In section 2 we introduce the model with the conditioned coupling constant $g(t)$ and perform the linearized stability analysis based on semiclassical equations of motion; in section 3 we visualize and discuss the results and also go beyond the linear stability analysis and give more details on the numerical procedure; in section 4 we summarize our findings, discussing them in a more general context.

2. Nonequilibrium Dicke model with time delayed feedback

2.1. Model

The Hamiltonian of the Dicke model

$$H = \omega \hat{a}^\dagger \hat{a} + \omega_0 \hat{J}_z + \frac{g(t)}{\sqrt{2j}}\left(\hat{a}^\dagger + \hat{a}\right)\left(\hat{J}_+ + \hat{J}_-\right) \tag{1}$$

describes the interaction between a single bosonic mode (with frequency ω and annihilation operator $\hat{a}$) and N two-level systems (with level splitting ω_0 and collective angular momentum operators $\hat{J}_{z,\pm}$) with total angular momentum $j = N/2$ [17]. We set the length of the pseudo-spin j to its maximum value. We assume an interaction between the bosonic mode and the collective angular momentum with a time-dependent coupling $g(t)$ that is modulated by a time-delayed feedback loop. Among various models for $g(t)$, the Pyragas form [5]

$$g(t) = g_0 + \frac{\lambda}{N}\left(\langle \hat{a}^\dagger \hat{a}\rangle (t-\tau) - \langle \hat{a}^\dagger \hat{a}\rangle (t)\right) \tag{2}$$

with the time-delayed feedback of the boson number at two different times t and $t-\tau$ and feedback strength λ turns out to lead to the richest phase diagrams. In the pioneering experiments (more details are in 4.1) for the Dicke–Hepp–Lieb phase transition in open photonic cavities [11], the form equation (2) would correspond to measured, average photon fluxes (proportional to the mean cavity photon occupation number [22, 23]) coupled back to a pump laser. Apart from the Pyragas delay form, this scheme is in fact close to the original feedback loops used for modulating the photon counting statistics in lasers [24].

We note that by using mean (expectation) values in equation (2) instead of operators (and additional noise terms in a stochastic master equation [25]) for the boson occupations, we already assume a mean field description that we expect to hold for $N \to \infty$ and that we formalize in the following.

2.2. Semiclassical equations

In analogy with semiclassical laser theory, phase transitions in the Dicke model for $N \to \infty$ are well described by mean-field equations for (factorized) operator expectation values [23, 26–28], which we denoted by the corresponding symbols without hat. Splitting a and $J_\pm$ into real and imaginary parts, $a = x + \mathrm{i}y$ and $J_\pm = J_x \pm \mathrm{i}J_y$, these equations read

$$\dot{x} = -\kappa x + \omega y, \quad \dot{y} = -\kappa y - \omega x - 2\frac{g(t)}{\sqrt{2j}}J_x, \tag{3}$$

$$\dot{J}_x = -\omega_0 J_y, \quad \dot{J}_y = \omega_0 J_x - 4\frac{g(t)}{\sqrt{2j}}\cdot x \cdot J_z, \dot{J}_z = 4\frac{g(t)}{\sqrt{2j}}\cdot x \cdot J_y,$$

where κ is decay rate of the bosonic mode and where the coupling $g(t)$ takes the form $g(t) = g_0 + \lambda\left(x_\tau^2 - x^2 + y_\tau^2 - y^2\right)$ with the shorthand $f_\tau \equiv f(t-\tau)$. Note that the angular momentum is a conserved quantity even for time dependent $g(t)$, and the time development therefore takes place on the surface of a Bloch sphere with the radius $N/2$. For zero time-delay $\tau = 0$, i.e., without feedback, the phase diagram is well known [27]. For $g < g_c \equiv \sqrt{\omega_0(\kappa^2+\omega^2)/4\omega}$, a stable normal phase solution corresponds to fixed point

$$J_x^0 = J_y^0 = x^0 = y^0 = 0,\ J_z^0 = -N/2, \tag{4}$$

whereas

$$J_x^0 = \pm\sqrt{\frac{N^2}{4} - J_z^{0^2}},\ J_y^0 = 0,\ J_z^0 = \frac{-N\omega_0\left(\kappa^2+\omega^2\right)}{8g_0^2\omega},$$

$$x^0 = -J_x^0\frac{2g_0\omega}{\sqrt{N}\left(\kappa^2+\omega^2\right)},\ y^0 = \frac{\kappa x_0}{\omega} \tag{5}$$

corresponds to the stable superradiant phase that exists only if $g \geqslant g_c$.

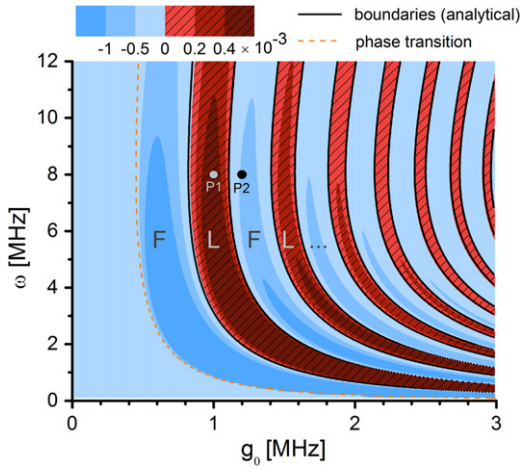

Figure 1. Phase diagram for fixed time delay τ and feedback strength λ. The dashed (orange) line separates the normal from the superradiant phase. The superradiant regime is split by time-delayed control into zones with stable fixed points (F) and limit cycles (L) with boundaries (black curves) determined from equation (10). Colour encodes the largest real part of the eigenvalue. Parameters: $\tau = 20\,\mu$s, $\lambda = 5$ MHz, and $\omega_0 = 0.05$ MHz, $\kappa = 8.1$ MHz [11, 27].

2.3. Stability analysis and feedback

To find out how the time-delayed feedback affects the stability of the system, we linearize equation (3) around the fixed points. (These do not depend upon τ, since the feedback equation (2) vanishes in the steady state.) Using the usual procedure [29], the linearized equations read

$$\delta\mathbf{v}'(t) = \mathbf{B}\cdot\delta\mathbf{v}(t) + \mathbf{A}\cdot\delta\mathbf{v}(t-\tau) \tag{6}$$

with $\delta\mathbf{v} = (\delta J_x,\ \delta J_y,\ \delta x,\ \delta y)^T$ describing the deviation from the fixed point and

$$\mathbf{A} = \frac{1}{N\sqrt{N}}\begin{pmatrix} 0 & 0 & 0 & 0 \\ 0 & 0 & -8J_z^0 x^{0^2}\lambda & -8J_z^0 x^0 y^0 \lambda \\ 0 & 0 & 0 & 0 \\ 0 & 0 & -4J_x^0 x^0\lambda & -4J_x^0 y^0\lambda \end{pmatrix},$$

$$\mathbf{B} = \begin{pmatrix} 0 & -\omega_0 & 0 & 0 \\ \dfrac{4g_0 J_x^0 x^0}{J_z^0\sqrt{N}} + \omega_0 & 0 & 8J_z^0 x^{0^2}\dfrac{\lambda}{N\sqrt{N}} - 4\dfrac{g_0}{\sqrt{N}}J_z^0 & 8J_z^0 x^0 y^0 \dfrac{\lambda}{N\sqrt{N}} \\ 0 & 0 & -\kappa & \omega \\ -2\dfrac{g_0}{\sqrt{N}} & 0 & 4J_x^0 x^0\dfrac{\lambda}{N\sqrt{N}} - \omega & 4J_x^0 y^0\dfrac{\lambda}{N\sqrt{N}} - \kappa \end{pmatrix}. \tag{7}$$

Note that the J_z component is determined by the conservation of angular momentum. Using the ansatz $\delta\mathbf{v} = \delta\mathbf{v}\,\mathrm{e}^{\Lambda t}$, we obtain the characteristic equation

$$\det\left(\Lambda\mathbf{1} - \mathbf{B} - \mathbf{A}\mathrm{e}^{-\Lambda\tau}\right) = 0. \tag{8}$$

For $\tau \neq 0$, this transcendental equation has an infinite set of solutions for the eigenvalues $\Lambda \in \mathbb{C}$. The fixed point $\mathbf{v}^0$ is stable if the real parts of all solutions Λ are negative, in which case the fluctuations decay to zero for $t \to \infty$.

3. Results

3.1. Phase diagrams

We obtain the phase diagram of our model in the ω–g_0–plane (figure 1) from the numerical solution of equation (8) for Λ. In all plots, the parameters are taken close to the experimental realization [11, 27]. We use 1600 different initial conditions for $\Lambda_0 = a_0 + ib_0$ ($a_0,\ b_0 \in [-40,\ 40]$) in the root-search algorithm in order to obtain all solution branches. The colour in figure 1 then encodes the maximum real part of all solutions Λ for a given system configuration.

First, in the left part of the phase diagram (for $g_0 \leqslant g_c$) we recover the usual normal phase, where the boson occupation is zero and, as a consequence, the feedback scheme equation (2) remains without effect. In contrast, for $g_0 > g_c$ and positive τ, the superradiant phase splits up into an infinite sequence of tongue-like areas that

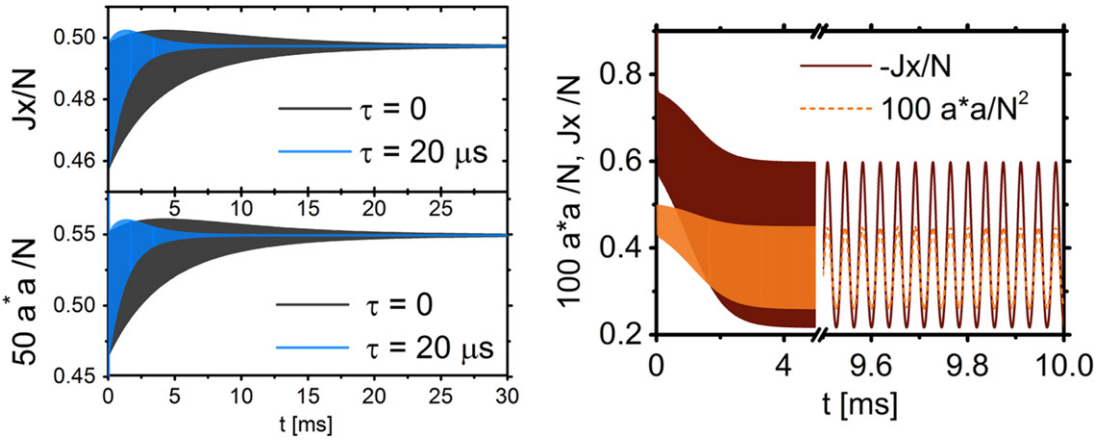

Figure 2. Time evolution of mode occupation a^*a and angular momentum component J_x corresponding to stable fixed point P2 (left) and stable limit cycle P1 (right) in the phase diagram figure 1.

alternate between zones with stable, superradiant fixed points (F), and—as we will see later—*limit cycles* (L) with periodically oscillating system observables. We will devote the rest of this paper to analysing and interpreting this rather surprising effect.

Figure 2 displays the two markedly different types of time evolution in the superradiant regime: in the fixed-point zones (F), the only effect of the Pyragas scheme is to speed up the convergence of the spin-components and the mean boson occupation a^*a towards their fixed-point values. This has to be contrasted with the limit-cycle zones (L), where the fixed point is unstable, and the observables end up oscillating with a single frequency. Therefore the system of coupled time-delayed differential equation (3) is solved numerically. We have to specify not only the initial conditions but also the history for $t \in [-\tau, 0]$, keeping it constant at the initial condition values. In all simulations we keep the values for $x(0)$ and $y(0)$ fixed around $0.1/\sqrt{N}$, set $J_y(0) \cdot N = 0$, and change the initial conditions for $J_z(0)$ or $J_x(0)$, respectively.

3.2. Analysis of zone boundaries

We obtain a simplified transcendental stability equation from equation (8) in the limit of very small level splitting $\omega_0 \ll \omega, g_0$, which describes the ultra-strong coupling limit of the Dicke model [30] and corresponds to a feedback-controlled displaced harmonic oscillator. However, this assumption is valid in the existing experimental setups [11, 27]. In this case, the angular momenta deviations $\delta J_{x,y}$ decouple from the field deviations δx, δy and describe periodic oscillations with the frequency

$$\Omega = \frac{4g_0^2\omega}{\kappa^2 + \omega^2}. \tag{9}$$

Using equation (8), we derive an equation for $\delta\ddot{x}$ just by inserting the equations into each other (see for details appendix A). As a result, we obtain

$$\tan\left(\frac{\Omega\tau}{2}\right) = \frac{-C_2 \pm \sqrt{-C_1^2 + C_2^2 + C_3^2}}{C_1 + C_3}, \tag{10}$$

with $C_1 = 2\kappa\Omega + \frac{2\lambda\kappa}{g_0\omega}\Omega^2, C_2 = 2g_0\lambda, C_3 = \frac{\lambda\kappa}{2g_0\omega}\Omega^2$, which leads to the roots of the equation (8) with a vanishing real part, i.e., $\Lambda = \pm i\Omega$. Parameter configurations satisfying this equation mark the boundary between stable (F) and unstable (L) fixed points, which is included in figure 1 and matches the numerically determined boundaries very well.

This analysis also allows us to elucidate the role of the delay time τ in the control scheme: to obtain real-valued results for the time delay τ, the root in equation (10) has to be positive. This condition is only satisfied if the feedback coupling λ is larger than some critical value λ_l, which we determine from the vanishing of the root in equation (10). We corroborate these findings by plotting the largest real part of the eigenvalue numerically determined from equation (8) in the (λ, τ)-plane for fixed ω and g_0 values (see figure 3). We recognize tongue-like zones switching between stable fixed-point and limit cycle (L) zones upon modification of the time delay τ and, furthermore, the existence of a critical feedback strength λ_l for entering in the (L) zones.

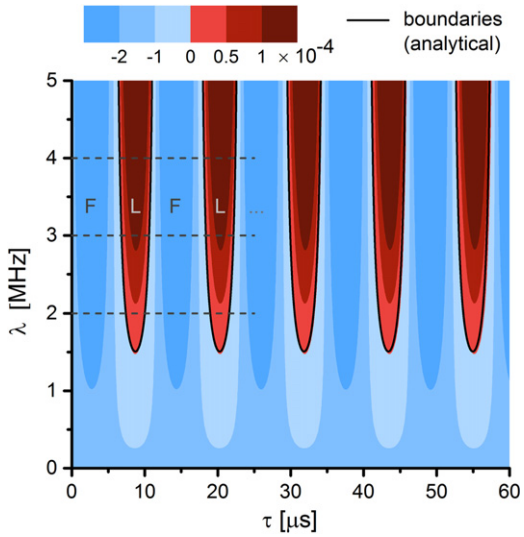

Figure 3. Phase diagram with sequence of stable fixed point (F) and limit cycle (L) zones in the λ (coupling strength) versus τ (delay time) plane. The black lines represent zone boundaries derived from the single trancendental equation (8). Dashed lines indicate cross-sections, shown in figure 4. Colour represents the largest real part of the eigenvalues. Parameters: $\omega = 10$ MHz, $g_0 = 1.5$ MHz, $\omega_0 = 0.05$ MHz, and $\kappa = 8.1$ MHz.

3.3. Limit cycle properties

Finally, we discuss the delay time τ and its role as a control parameter. Therefore we solve the equations of motion (3), keeping all parameters except τ at fixed values. Increasing the time delay τ, we cross the boundary and switch into the (L) zone of the corresponding phase diagram (figure 3). This is accompanied by a stability swap; the fixed point becomes unstable, and a stable limit cycle appears. This is known as a supercritical Hopf bifurcation. Figure 4 (upper panel) visualizes this behaviour, showing the time evolution of the atom-subsystem on the Bloch sphere for two different τ-values. Instead of plotting the typical Hopf bifurcation diagram by using absolute values (figure 4, lower left), we show the equivalent representation by plotting only the radius (amplitude) of the emerging limit cycle as a function of time delay τ (figure 4, lower right). Zero amplitude would correspond to a stable fixed point. Note that, due to the parity invariance $x \to -x$, $y \to -y$, $J_x \to -J_x$, $J_y \to -J_y$ of equation (3), there are not only two fixed points in the superradiant regime but also two stable limit cycles with the same amplitude if τ matches the (L) zone. This bifurcation diagram does not distinguish between the two limit cycles, as we plot only relative values and they are the same for both limit cycles.

Solving the equations of motion (3) for parameter values along the dashed lines in figure 3, we find that the amplitude and period T of the limit cycles depend upon τ, as depicted in figure 5 for the J_z amplitude. First, we recognize that for initial conditions close to the fixed point (typically we use $J_z(0) = 0$ or $(J_z(0) - J_z^0)/J_z^0 \approx 0.1\%$ as initial conditions), both the amplitude and the period show the same Hopf bifurcation scenario (connected lines) appearing for certain values of τ. The non-zero slope of the curves marks the beginning of the L-zone and the Hopf bifurcation; the maxima of the curves mark the end of the L-zone. As a particularly striking feature, we observe a drastic collapse of the limit cycle (vertical lines) for values of $\lambda > \lambda_l$ and the birth of an unstable limit cycle (disconnected unfilled symbols, shown only in the upper part of figure 5) by a subcritical Hopf bifurcation when the time delay τ reaches the end of the (L) zone. Our numerics show that this collapse occurs as a jump discontinuity. Furthermore, a stable limit cycle still exists behind the (L) zone (disconnected filled symbols) as a continuation of the previous one, but, because of bistability with the stable fixed point, it can only be reached if the initial amplitude lies above the amplitude of the unstable limit cycle, which marks the boundary between the basins of attraction of the fixed point and limit cycle attractors. The branches of the stable and the unstable limit cycles merge in a saddle-node-bifurcation (arrows in figure 5). The inset shows this bifurcation schematically. The dotted arrows point to the stable solution (black solid line) that the system will take for different initial conditions. Note that, to assess the amplitude of the unstable limit cycle, we change the initial condition $J_z(0) \cdot N \in [0.5, -0.5]$ in small steps $\delta J_z(0)$ until the solution converges to the other attractor. Then we identify the initial amplitude of $J_z(t)$ with the amplitude of the unstable limit cycle, which is a good approximation for small $\delta J_z(0)$.

In addition, the theoretical prediction for the oscillating frequency Ω from the linear stability analysis of the fixed-point equation (9) matches well with the damped oscillation period in the F-region (see figure 5). The

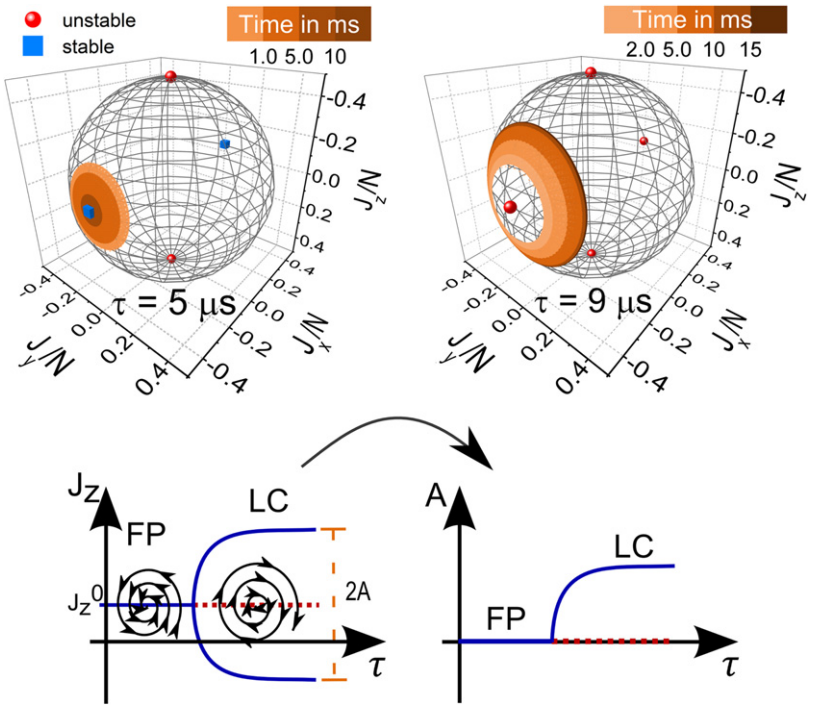

Figure 4. Time evolution of the spin component for two different time delays τ corresponding to stable fixed point and stable limit cycle, respectively (upper panel). A sketch of the Hopf bifurcation scenario by plotting the J_z values of fixed point (FP) and the max/min J_z-value of the limit cycle (LC) and the corresponding amplitude representation (lower panel). Parameters: as in figure 3, $\lambda = 3$ MHz.

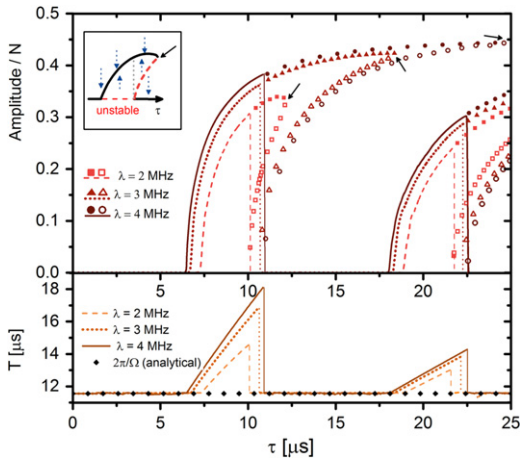

Figure 5. Bifurcation scenario for limit-cycle amplitudes (upper) and periods T (lower) of J_z as a function of delay time τ along the cross-sections (dashed lines at fixed λ) in figure 3. The filled symbols in the upper part describe the continuation of the limit cycle for initial value above the unstable limit cycle (unfilled symbols). The inset sketches the appearing saddle-node bifurcation of limit cycles, and the dotted arrows show the direction of the phase flow for fixed tau.

mean occupation of the optical mode $a^\star a$—as all $\mathbf{v}$ components—shows the same oscillating behaviour. As a consequence of $a^\star a$ being proportional to the photon output, the mean number of photons emitted from the system also oscillates with a fixed frequency that can be externally controlled.

4. Discussion

The application of the Pyragas control to the coupling g of the Dicke model generates a complex phase diagram with stable fixed points (F) and limit cycles (L) in the superradiant regime. The alternations between (F) and (L) zones (figure 3) in fact constitute an infinite sequence of super- and subcritical Hopf bifurcations of the

stationary state generating stable and unstable limit cycles, respectively. Furthermore, the feedback generates bistable regions ending by a saddle-node bifurcation.

4.1. Experimental *realization*

In the experimental setup [11], a Bose–Einstein condensate (BEC) is trapped inside an optical cavity and is additionally driven by a pump laser. The two-level atomic system is built of atoms with two different momentum states, where one is the BEC ground state. Other momentum states have to be excluded by a two-mode assumption, which is fulfilled if the pumping frequency is far detuned from the resonant atomic frequencies. The collective spin operators $J_{\pm}$ describe the atomic transitions in the collective momentum space. The interaction term in the Dicke–Hamiltonian (1) is an effect of the interplay between the photons of the pumping field and the cavity photons via the two-level system. Furthermore, equation (1) is given in the rotating frame at the pump laser frequency. In that way, the Hamiltonian has no direct dependence on the pumping laser; its properties are already included in the parameters. Thus the coupling constant g, which becomes time-dependent in our approach, is defined by the light intensity of the pumping field.

On the one hand, our approach modifies only this intensity and does not add additional frequencies to the cavity. The intensity increase/decrease is small compared to the uncontrolled system, because $g_0 \ll \lambda/Na^{\star}a$, as we can conclude from figure 2, and λ can be assumed to be unity to achieve the calculated effects (see figure 3). Thus, the two-mode approximation of the Dicke model in the atomic momentum space should remain valid, and no other energy states except these two should be excited. On the other hand, it should be possible to restrict the feedback strength parameters such that the possible excitations are avoided.

Deviations due to photon loss between the measured mean photon number and its actual value can be compensated by time interval extension for calculating the mean value (because of rather slow dynamical evolution with fast oscillations) or by tuning the λ-coupling.

4.2. Aspects of Pyragas control

The open loop control provided in [18] creates new fixed points in the normal and superradiant regime, so a bifurcation is induced by periodic modulation of the coupling constant. In contrast, the closed loop control scheme used here completely changes the impact on the Dicke system and the bifurcation scenario. Although the Pyragas control performed by Grimsmo *et al* [21] is physically very different from our scheme, it creates similar phase diagrams with limit cycles. Furthermore, adding the back action of the cavity field $U\hat{J}_z\hat{a}^{\dagger}\hat{a}$ to the Dicke–Hamiltonian H equation (1), there are some parameter regimes where the solution of the mean-field equation has persistent oscillations [27]. This is linked to the absence of stable fixed points; the same happens in the LC-zone and is caused by time delay. These analogies indicate that the analysed limit cycle phase is not something that is artificially added to the model by Pyragas control. Rather, this phase is hidden in the model and becomes visible by the control. We remark that the possibility of periodic dynamics in such systems was also observed in optomechanical BEC experiments [31, 32].

We emphasize that the time dependence of $g\,(t \to \infty)$ (equation (2)), does not disappear in the L-regions, in contrast to the F-regions, leading to the phase diagram discussed above. In the L-region, $g(t)$ oscillates with the same period as the other system observables. This is a consequence of subtracting two oscillating functions $x\,(t-\tau)^2 + y\,(t-\tau)^2$ and $x\,(t)^2 + y\,(t)^2$ with the same period. Our feedback scheme here switches between non-invasive and invasive behaviour by crossing the boundaries within the phase diagram. Our results also demonstrate that the Pyragas form in equation (2) is essential to create a new stable phase. In contrast, for the direct feedback scheme $g\,(t) = g_0 + \lambda\,\langle\hat{a}^{\dagger}\hat{a}\rangle\,(t-\tau)$, depending on parameter values, the occupation of the optical mode diverges, and the control does not work well, or the time delay does not seriously modify the phase diagram at all (not shown here).

Finally, we also checked that the (experimentally less practical) Pyragas feedback for the angular momentum (instead of the photonic feedback) also leads to the creation of a limit-cycle phase in the superradiant regime but cannot influence the stability of the normal phase.

We expect that our feedback scheme can be implemented whenever semiclassical equations of motion provide an adequate description for the quantum bifurcation-type phase transitions that govern models with collective degrees of freedom, such as the Dicke or the Lipkin–Meshkov–Glick model [33].

An open and challenging problem is the implementation of time-delayed feedback control for quantum critical systems beyond the mean-field level, i.e., where quantum fluctuations are expected to play a major role [34].

Acknowledgments

We thank H Aoki, J Lehnert, and N Tsuji for useful discussions. The authors gratefully acknowledge financial support from the DAAD and DFG Grants BR 1528/7–1, 1528/8–2, 1528/9–1, SFB 910, and GRK 1558.

Appendix. Boundaries

In the case of $\omega_0 \to 0$, the superradiant fixed-point solutions can be approximated as

$$J_z^0 \to 0,\ J_x^0 \to \pm\frac{1}{2}N,\ x^0 \to -\frac{2g_0\omega}{\sqrt{N}\left(k^2+\omega^2\right)}J_x^0,\ y^0 \to \frac{k}{\omega}x^0. \tag{A.1}$$

The linearized equation (6) for the fluctuations $\delta\mathbf{v}$ becomes, then,

$$\delta\mathbf{v}'(t) = \mathbf{B_0}\cdot\delta\mathbf{v}(t) + \mathbf{A_0}\cdot\delta\mathbf{v}(t-\tau), \tag{A.2}$$

$$\mathbf{A_0} = \frac{1}{N\sqrt{N}}\begin{pmatrix} 0 & 0 & 0 & 0\\ 0 & 0 & 0 & 0\\ 0 & 0 & 0 & 0\\ 0 & 0 & -4J_x^0x^0\lambda & -4J_x^0y^0\lambda \end{pmatrix},$$

$$\mathbf{B_0} = \begin{pmatrix} 0 & -\omega_0 & 0 & 0\\ \Omega^2/\omega_0 & 0 & 0 & 0\\ 0 & 0 & -\kappa & \omega\\ -2\dfrac{g_0}{\sqrt{N}} & 0 & 4J_x^0x^0\dfrac{\lambda}{N\sqrt{N}}-\omega & 4J_x^0y^0\dfrac{\lambda}{N\sqrt{N}}-\kappa \end{pmatrix}$$

with $\Omega^2 = \frac{4g_0J_x^0x^0\omega^0}{J_z^0\sqrt{N}}$.

Using $\delta\vec{v} = (\delta J_x,\ \delta J_y,\ \delta x,\ \delta y)^T$, we see first that

$$\left.\begin{aligned}\delta\dot{J}_x &= -\omega_0\delta J_y\\ \delta\dot{J}_y &= \frac{\Omega^2}{\omega_0}\delta J_x\end{aligned}\right\} \Rightarrow \delta\ddot{J}_x = -\Omega^2\delta J_x.$$

From equation (A.2) we get

$$\begin{aligned}0 = {}&\delta\ddot{x} + 2\kappa\delta\dot{x} + \left(\omega^2+\kappa^2\right)\delta x - 2g_0\lambda\left(\delta x_\tau - \delta x\right)\\ &-\frac{2\dfrac{\lambda}{N\sqrt{N}}\kappa\sqrt{g_0}\sqrt{N}}{\omega^2+\kappa^2}\left(\delta\dot{x}_\tau - \delta\dot{x}\right) + 2\sqrt{g_0}\sqrt{N}\omega\delta J_x.\end{aligned} \tag{A.3}$$

Applying an additional time derivative and inserting then the two upper equations into each other, we obtain

$$\begin{aligned}0 = {}&\delta\dddot{x} + 2\kappa\delta\ddot{x} + \left(\omega^2+\kappa^2\right)\delta\dot{x} + 2\frac{g_0}{\sqrt{N}}\omega\delta\dot{J}_x\\ &+4\frac{\lambda}{N\sqrt{N}}J_x^0\Big(\left(\omega x^0 + ky^0\right)\left(\delta x_\tau - \delta x\right) + y^0\left(\delta\dot{x}_\tau - \delta\dot{x}\right)\Big).\end{aligned} \tag{A.4}$$

By use of the superradiant fixed-point solutions equation (A.1), it can be shown that

$$4\frac{\lambda}{N\sqrt{N}}J_x^0\left(\omega x^0 + ky^0\right) = -2\lambda g_0, \tag{A.5}$$

$$4\frac{\lambda}{N\sqrt{N}}J_x^0y^0 = -\frac{2g_0\lambda\kappa}{\kappa^2+\omega^2},\ \Omega = \frac{4g_0^2\omega}{\left(\kappa^2+\omega^2\right)}.$$

This simplifies equation (A.4) to

$$\begin{aligned}0 = {}&\delta\ddot{x} + 2\kappa\delta\dot{x} + \left(\omega^2+\kappa^2\right)\delta x - 2g_0\lambda\left(\delta x_\tau - \delta x\right)\\ &-\frac{2\lambda\kappa g_0}{\omega^2+\kappa^2}\left(\delta\dot{x}_\tau - \delta\dot{x}\right) + 2\frac{g_0}{\sqrt{N}}\omega\delta J_x.\end{aligned} \tag{A.6}$$

Inserting the ansatz $\delta J_x = E_1 \sin(\Omega t)$, $\delta x = E_2 \sin(\Omega t)$ into this differential equation, we obtain the following condition for its validity

$$0 = C_1 + C_2 \cdot \sin(\Omega\tau) - C_3 \cos(\Omega\tau) \tag{A.7}$$

with C_i defined in equation (10). Using the connections $\sin(x) = \frac{2\tan(x/2)}{1+\tan^2(x/2)}$, $\cos(x) = \frac{1-\tan^2(x/2)}{1+\tan^2(x/2)}$, the upper expression can be rewritten as equation (10).

This expression determines the boundaries between the (F) and (L) zones in the phase diagrams. Note that the ansatz assumes that the the eigenvalues of equation (8) have no real parts. That means that $\Lambda = \mathrm{i}\Omega$ and the components of $\mathbf{v}$ oscillate undamped with fixed frequency if the linear approximation near the fixed point is valid.

References

[1] Lignier H, Sias C, Ciampini D, Singh Y, Zenesini A, Morsch O and Arimondo E 2007 *Phys. Rev. Lett.* **99** 220403
[2] Kinoshita T, Wenger T and Weiss D S 2006 *Nature* **440** 900
Hofferberth S, Lesanovsky I, Fischer B, Schumm T and Schmiedmayer J 2007 *Nature* **449** 324–7
[3] Eckstein M, Kollar M and Werner P 2009 *Phys. Rev. Lett.* **103** 056403
[4] Caprio M A, Cejnar P and Iachello F 2008 *Ann. Phys.* **323** 1106
[5] Pyragas K 1992 *Phys. Lett.* A **170** 421–8
[6] Schöll E and Schuster H G 2008 *Handbook of Chaos Control* (New York: Wiley)
[7] Choe C-U, Jang H, Flunkert V, Dahms T, Hövel P and Schöll E 2013 *Dynamical Systems* **28** 15–33
[8] Flunkert V, Yanchuk S, Dahms T and Schöll E 2010 *Phys. Rev. Lett.* **105** 254101
[9] Schöll E 2013 *Advances in Analysis and Control of Time-Delayed Dynamical Systems* ed J-Q Sun and Q Ding (Singapore: World Scientific) ch 4 pp 57–83
[10] Dicke R H 1954 *Phys. Rev.* **93** 99–110
Wang Y K and Hioe F T 1973 *Phys. Rev.* A **7** 831–6
Hepp K and Lieb E H 1973 *Ann. Phys.* **76** 360–404
[11] Baumann K, Guerlin C, Brennecke F and Esslinger T 2010 *Nature* **464** 1301
[12] Ritsch H, Domokos P, Brennecke F and Esslinger T 2013 *Rev. Mod. Phys.* **85** 553
[13] Baumann K, Mottl R, Brennecke F and Esslinger T 2011 *Phys. Rev. Lett.* **107** 140402
[14] Nagy D, Kónya G, Szirmai G and Domokos P 2010 *Phys. Rev. Lett.* **104** 130401
[15] Klinder J, Keßler H, Wolke M, Mathey L and Hemmerich A 2014 arXiv 1409.1945
[16] Baden M P, Arnold K J, Grimsmo A L, Parkins S and Barrett M D 2014 *Phys. Rev. Lett.* **113** 020408
[17] Emary C and Brandes T 2003 *Phys. Rev.* E **67** 066203
Emary C and Brandes T 2003 *Phys. Rev. Lett.* **90** 044101
[18] Bastidas V M, Emary C, Regler B and Brandes T 2012 *Phys. Rev. Lett.* **108** 043003
[19] Vacanti G, Pugnetti S, Didier N, Paternostro M, Palma G M, Fazio R and Vedral V 2012 *Phys. Rev. Lett.* **108** 093603
[20] de Liberato S, Gerace D, Carusotto I and Ciuti C 2009 *Phys. Rev.* A **80** 053810
[21] Grimsmo A L, Parkins A S and Skagerstam B S 2014 *New J. Phys.* **16** 065004
[22] Öztop B, Bordyuh M, Müstecaploglu E and Türeci H E 2012 *New J. Phys.* **14** 085011
[23] Kopylov W, Emary C and Brandes T 2013 *Phys. Rev.* A **87** 043840
[24] Machida S and Yamamoto Y 1986 *Opt. Commun.* **57** 290–6
[25] Wiseman H M and Milburn G J 2010 *Quantum Measurement and Control* (Cambridge: Cambridge University Press)
[26] Bonifacio R and Preparata G 1970 *Phys. Rev.* A **2** 336
[27] Bhaseen M J, Mayoh J, Simons B D and Keeling J 2012 *Phys. Rev.* A **85** 013817
[28] Armen M A and Mabuchi H 2006 *Phys. Rev.* A **73** 063801
[29] Hövel P and Schöll E 2005 *Phys. Rev.* E **72** 046203
[30] Aparicio A M, Bucher M, Emary C and Brandes T 2012 *Phys. Rev.* E **86** 012101
[31] Ritter S, Brennecke F, Baumann K, Donner T, Guerlin C and Esslinger T 2009 *Appl. Phys.* B **95** 213–8
[32] Brennecke F, Ritter S, Donner T and Esslinger T 2008 *Science* **322** 235–8
[33] Lipkin H J, Meshkov N and Glick A J 1965 *Nuclear Phys.* **62** 188–98
[34] Nagy D, Szirmai G and Domokos P 2011 *Phys. Rev.* A **84** 043637